



Article

Attachment of Fibrinogen on Ion Beam Treated Polyurethane

Vyacheslav Chudinov ¹, Igor Shardakov ¹, Irina Kondyurina ^{2,3} and Alexey Kondyurin ^{3,4,*}

¹ Institute of Continuous Media Mechanics, Ural Branch, Russian Academy of Sciences, Perm 614013, Russia; chudinovsl@mail.ru (V.C.); shardakov@icmm.ru (I.S.)

² School of Medicine, University of Sydney, Camperdown, NSW 2050, Australia; i.kondyurina@gmail.com

³ Ewingar Scientific, Ewingar, NSW 2469, Australia

⁴ School of Physics, University of Sydney, Camperdown, NSW 2050, Australia

* Correspondence: kond@mailcity.com

Abstract: Protein-stable coverage of the artificial implant is a key problem for biocompatibility. In the present study, a protein layer was attached covalently to a polyurethane surface treated by an ion beam. A plasma system consisting of a vacuum chamber (0.8 Pa pressure) with a high voltage electrode powered by a short pulse (20 μ S pulse duration and 200 Hz pulse repetition) generator was designed. Polyurethane with a formulation certified as a material for medical implants was treated by nitrogen ions with an energy of 20 keV and 5×10^{14} – 10^{16} ions/cm² fluence range. Wettability measurements, X-ray photoelectron, Raman, Fourier transform infrared attenuated total reflection, and ellipsometry spectra showed a significant change in the structure of the surface layer of the treated polyurethane. The surface of the treated polyurethane contained a carbonised layer containing condensed aromatic clusters with terminal free radicals. The surface energy of polyurethane surface increased from 33 to 65 mJ/m². The treated polyurethane surface became capable of adsorbing and chemically binding protein (fibrinogen). The designed system for ion beam treatment can be used for surface activation of biomedical polymer devices, where a total protein coverage is required.

Keywords: protein; covalent attachment; polyurethane; ion beam treatment



Citation: Chudinov, V.; Shardakov, I.; Kondyurina, I.; Kondyurin, A.

Attachment of Fibrinogen on Ion Beam Treated Polyurethane.

Biomimetics **2024**, *9*, 234. <https://doi.org/10.3390/biomimetics9040234>

Academic Editor: Xiang Ge

Received: 6 March 2024

Revised: 8 April 2024

Accepted: 12 April 2024

Published: 15 April 2024



Copyright: © 2024 by the authors. Licensee MDPI, Basel, Switzerland. This article is an open access article distributed under the terms and conditions of the Creative Commons Attribution (CC BY) license (<https://creativecommons.org/licenses/by/4.0/>).

1. Introduction

The nonspecific interaction of the surface of a biomedical device with molecules from an organism or a biotechnological process is a constant obstacle to the use of artificial materials in biomedical technologies [1–3]. This interaction leads to a change in the conformation of biologically significant molecules and their activity, disrupting their bio functionality [4,5]. The best way out of this problem is to modify the surface of an artificial material by applying a permanently bound total layer of biological molecules on the surface while preserving their conformation and activity [6–9].

In some cases, it can be achieved by using precursor intermediate molecules, with one side attached to the surface of the device and the other providing a covalent attachment of the protein to the surface [10–14]. There are a number of publications where the surface of a polymer implant was treated for chemical binding with protein. For example, some applications involving protein attachment have achieved success by utilising linkers such as cysteamine [15], N-hydroxysuccinimide, N-(3-dimethylaminopropyl)-N'-ethyl carbodiimide hydrochloride [16,17], glutaraldehyde [18–23], succinimidyl 3-(2-pyridyldithio)propionate and 2-pyridylthio benzophenone PDT-BzPh photolinker [24]. These surface preparation methods are convenient for protein attachment. However, toxic reagents have to be used, which is undesirable for biomedical implants of organisms. In addition to that, the covalently attached protein covers only a part of the implant surface, but complete surface coverage is required. Therefore, in some cases, the use of these precursors is unacceptable.

As was shown in some cases, plasma activation of the surface and direct covalent grafting of the protein and other molecules can be used without any precursors. For

this purpose, ion beam treatment methods were used for polymer implants, plasma immersion ion implantation (PIII), and plasma polymerisation methods. These are very powerful methods that cause carbonisation, oxidation, and depolymerisation of the thin surface layer of different polymers while preserving the bulk underneath layers [25–36], including polyurethanes (PUs) [32–42]. Some examples of these systems are the ion beam implanter ILU [43], the ion beam implanter Pulsar at the Institute of Technical Chemistry in Perm [44,45], PIII systems at Rossendorf Research Center in Dresden [46] and Leibniz Institute of Surface Engineering in Leipzig [47], and PIII and plasma polymerisation systems at the University of Sydney [47].

The complete coverage of the surface with protein has been demonstrated, in particular, during plasma immersion implantation of a number of polymers. Proteins have been covalently attached to polyethylene (PE), polystyrene, polytetrafluorethylene, Nylon, polyvinyl chloride, polypyrrole, polycarbonate, polyether ether ketone, polyether sulfone, PUs, polycaprolactone, and polydimethyl siloxane without the use of a precursor. The following have been demonstrated to be covalently attached and maintain catalytic activity: poly-L-lysine and Catalase, Horseradish peroxidase, β -glucosidase, tropoelastin, collagen, fibronectin, poly-L-glycine, Poly-DL-alanine, Poly-L-isoleucine, poly-L-lysine, Poly-L-histidine, Poly-L-tryptophan, Poly-L-tyrosine, Poly-L-Threonine, Poly-L-methionine, osteocalcin, and antibodies CD2, CD3, CD29, CD184, CD244.1, CD326, and CD34. Additionally, covalently attached oligonucleotides have also been shown. In this case, the protein coating was applied to 92% of the polymer surface area. The remaining area of the surface (without the protein) was not accessible to the protein molecules due to steric hindrance caused by neighbouring molecules. Therefore, the polymer surface area can be considered fully covered (100%). Protein grafting onto the treated polymer surface is based on the reaction of free radicals located at the edges of graphite clusters on the polymer surface. The universality of free radical chemical activity allows the protein molecule to graft via any amino acid residue [48].

An example of successful protein grafting is the result of eliminating a foreign body reaction in an organism by implanting a PIII-activated PU implant in an animal. This implant shows a significantly weakened rejection reaction and, in some cases, the absence of a foreign body reaction [49]. The grafted protein hides the surface of the PU implant from the immune cells, and the organism does not recognise the implant as a foreign body. An analysis of the grafted proteins on the implant surface extracted from the animal showed the presence of a number of important functional proteins, such as collagen, fibrinogen, and others [50–54]. In the present study, we investigate the chemical attachment of fibrinogen to the surface of medical PU for implants.

For surface activation, the polymer must be treated with a high-energy ion beam. For this purpose, ion accelerators can be used. The polymer is placed in a vacuum chamber, and a high vacuum is created. Then, a plasma is formed separately, from which a beam of ions is extracted and accelerated. The ion beam can be separated from other particles by composition and energy. An ion accelerator is a fairly large and expensive machine. The area of the beam spot is about 1 cm². There are also accelerators without ion beam separation with a larger aperture, which allow processing polymer areas up to 100 cm² [55]. The ion beam in these systems is unidirectional, which limits the shape of the polymer being processed. The strong vacuum requirement in these systems limits the class of polymers processed, which must have a low rate of outgassing.

A more technologically advanced method is PIII [47,56]. The PIII technique involves placing a high-voltage electrode with a polymer in a vacuum chamber. The polymer is covered with a metal grid connected to a high-voltage electrode to exclude a changing effect [47]. The radio frequency or microwave plasma is generated in the chamber. A short high-voltage pulse is applied to the high-voltage electrode, which pulls ions out of the plasma and accelerates them in a direction perpendicular to the grid. The ions are accelerated through the grid and bombard the polymer. In this case, the grid and

the processed polymer can be of a complex shape [57]. This method is more suitable for processing real polymer implants used in medicine and biomedical technologies.

However, when PIII plasma is used in a vacuum chamber, the plasma cloud usually touches the walls of the chamber. As a result of plasma bombardment of the chamber walls, the wall material can be etched, and the chamber gas environment can be contaminated. The authors had these negative experiences. As a result, the products of etching of the chamber walls can approach the polymer surface being processed and deactivate it. In this case, the PIII could not activate the polymer surface, and chemical grafting of the protein could not be conducted. To eliminate this effect, it is desirable that the plasma in the chamber does not touch the chamber walls or other parts of the system.

As an option to eliminate the contact between the plasma and the chamber wall, we have designed a different ion beam implanter based on a different principle: no additional plasma is generated in the chamber, and a high-voltage pulse is applied only to the high-voltage electrode. Then, during a high-voltage pulse, plasma appears above the surface of the electrode, and at the same time, the ions are pulled out and accelerated toward the high-voltage electrode. With a sufficiently large space above the electrode, the plasma sheath does not reach the chamber walls, and the influence of the etching of the wall material is eliminated. The size of the electrode and, consequently, the area of the treated polymer is limited only by the volume of the vacuum chamber. The shape of electrodes and polymer implants can be complex. In addition, this eliminates the need to generate radio frequency or microwave plasma in the chamber, which simplifies the system design and makes its operation more stable. This new ion beam treatment method was tested in the present study.

2. Materials and Methods

In the experiments, polyurethane SKU-PFL, which is certified for medical use and long-term implants in the human body, was used [58–60]. PU was synthesised from polytetrahydrofuran with terminal hydroxyl groups terminated by toluene diisocyanate. MOCA aromatic diamine was used for curing. The formula of PU is shown in Figure 1. PU films 0.3 mm thick were prepared for this study. Before treatment, PU films were swollen in toluene to wash out unreacted products, and then the films were dried until the solvent was completely removed. The presence of solvent and unreacted products was monitored by FTIR ATR spectra and mass loss measurements.

The PU samples were treated in a plasma system consisting of a vacuum chamber, turbomolecular pump, scroll dry pump, and high-voltage pulse generator (Figure 1). The pressure was measured with a digital vacuum meter. The ultimate pressure of the residual atmosphere was down to 0.013 Pa (0.1 mTorr). The working pressure of nitrogen gas was 0.8 Pa (6 mTorr). The samples were placed on a high-voltage electrode and covered by a metal grid. High voltage pulses of -20 kV were applied. The pulse duration was 20 μ s, and the pulse frequency was 200 Hz. The pulse voltage and current were measured with digital oscilloscopes. The ion fluence was calibrated using UV spectra of the treated PE film following the method described in [47]. UV transmission spectra of PE films for the fluence calibration were recorded on a Varian spectrophotometer.

The treated PU samples were incubated in fibrinogen solution (20 g/L in a 10 mM sodium phosphate buffer, pH = 7) overnight at room temperature. Each sample was treated in an individual tube. After that, the samples were washed 6 times in a new tube and fresh buffer each time. Each wash in buffer was 10 min. After that, the samples were rinsed for a few seconds in mQ water to remove the buffer salts and were then dried overnight. For control, the untreated PU samples were incubated and washed under similar conditions. Other control-treated and untreated PU samples without protein were incubated only in buffer solution and rinsed in mQ water under similar conditions at the same time as the samples with protein. Then, the FTIR ATR spectra of all these samples were recorded.

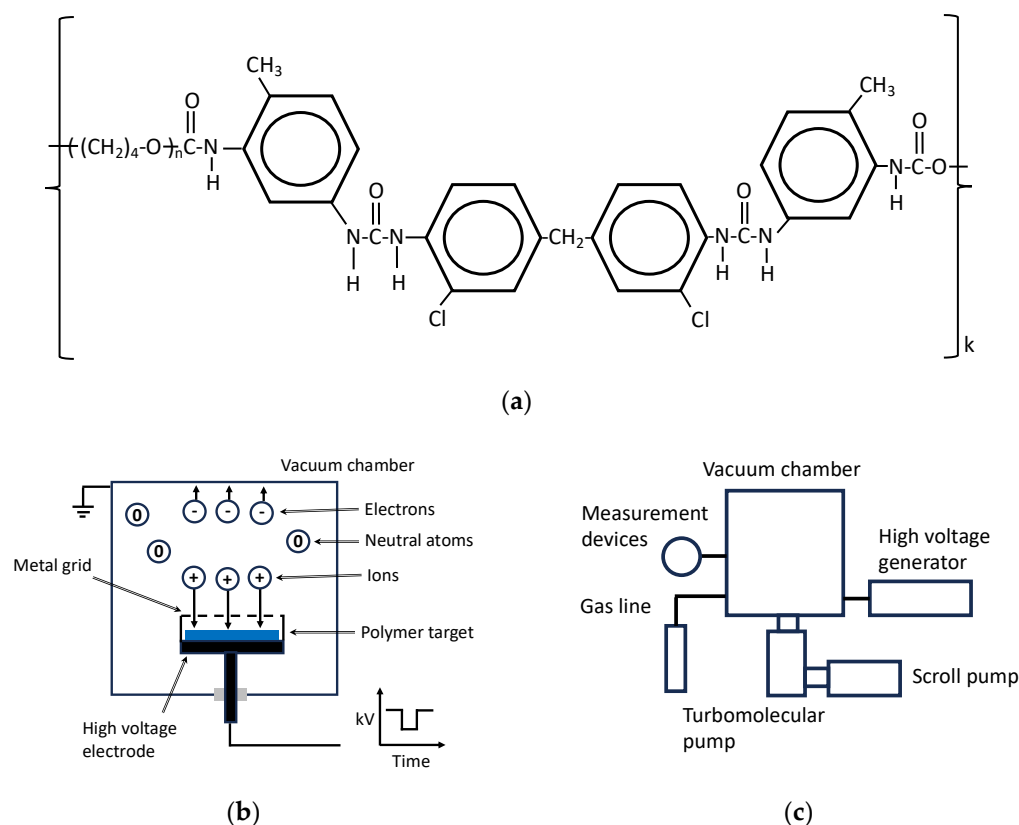


Figure 1. (a) The PU formula and (b,c) scheme of the plasma system. (b) The scheme of the plasma chamber with a high voltage electrode, grid, and polymer sample (blue rectangular). The plasma is generated during a short, high-voltage pulse. Ions from plasma are accelerated towards the polymer surface. (c) A block scheme of the system, including vacuum pumps, gas line, high voltage generator, and sensors of pressure, voltage, current, and plasma spectrum (marked as measurement devices).

After the spectra recording, all treated and untreated samples with and without protein were washed in sodium dodecyl sulphate (SDS) detergent solution of 2% at 70 °C for 2 h to remove all physically adsorbed protein. Each sample was washed in an individual tube. After that, the samples were washed in mQ water 3 times, each time in a new tube to remove the SDS detergent. Each sample was washed in an individual tube and then dried overnight. The FTIR ATR spectra of dried samples were recorded.

The samples were measured with the FTIR (Fourier transform infrared) spectrometer Digilab (Digilab, Hopkinton, MA, USA) equipped with an ATR (attenuated total reflection) accessory. The prism crystal of Ge with a 45-degree incident angle and 25 reflections was used as the ATR element. The 500 scans for each spectrum with a spectral resolution of 4 cm^{-1} were used. The surface layer of the samples was measured with a Woollam M2000V spectroscopic ellipsometer. The measurements were conducted for three angles, 65, 70, and 75 degrees, in a range of 200–1000 nm wavelength. The Cauchi layer was used for the optical model. The KRUSS contact angle analyser was used for water and diiodomethane contact angle measurements. The optical images of the sample surface were obtained using a Carl Zeiss Jena microscope with a digital camera. X-ray photoelectron (XPS) spectra were recorded using a SPECS spectrometer. Additionally, an Al K_{α} monochromatic X-ray source was used. Survey spectra in an eV region of 50–1400 eV and high-resolution spectra of C_{1s} , N_{1s} , and O_{1s} regions were recorded. The SRIM-2003 code was used to calculate ion penetration depth into the PU [61,62].

3. Results

3.1. Evaluation of Treatment Parameters

The choice of treatment regime was based on previously obtained results on the activation of the polymer surface during ion beam treatment in the Pulsar implanter and PIII systems. The treatment parameters of the new system were calibrated to obtain the same result as the PE film treatment. The maximum voltage of 20 kV was determined by previous successful polymer processing results. The shape of the high-voltage pulse was close to rectangular, which ensured, if possible, that only ions of a given energy were processed. Figure 2 shows diagrams of the voltage and current of the electrode at different pressures in the vacuum chamber. At ultimate pressure (0.1 mTorr) in the vacuum chamber, there was no plasma and a slow voltage drop after the end of the pulse was ensured due to the low discharge current in the electronic circuit of the pulse source. At pressure lower than 5.5 mTorr, no plasma current and slow discharge current were observed in the chamber. As the pressure increased, the discharge current pulse appeared at the end of the pulse. In this case, the voltage drop after the pulse occurred due to a gas discharge through the plasma formed during the pulse. When the pressure increased to 7.3 mTorr, the discharge current reached the maximum values provided by the high-voltage source. The shape of the voltage pulse became rectangular, showing a decrease in values at the end of the pulse. These measurements made it possible to select the working gas pressure with maximum processing efficiency and stable ion energy set by the voltage on the high-voltage electrode. Note that the main part of the ion current in this mode occurs at the end of each high-voltage pulse, ensuring the accelerating voltage's stability for all ions throughout the entire pulse.

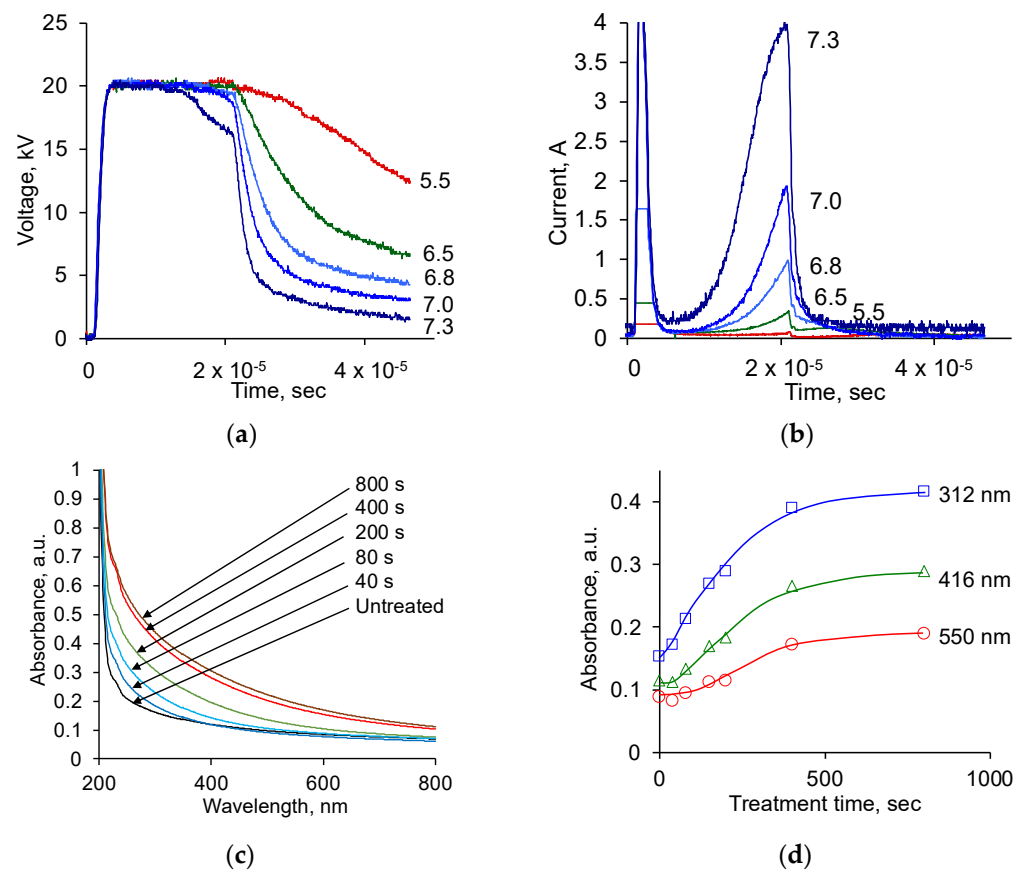


Figure 2. (a) Voltage oscillogram during pulses at different pressures (marked in mTorr) in a vacuum chamber; (b) current oscillogram during pulses at different pressures (marked in mTorr) in a vacuum chamber; (c) UV spectra of PE films treated for various durations (for fluence calculation) (see in text); (d) UV spectra absorbance of PE films at different wavelengths to determine the fluence of ion beam treatment (for fluence calculation) (see in text).

The pulse repetition frequency of 200 Hz was limited by the requirement that the polymer samples should not overheat. With an increase in the pulse repetition frequency, the PE film used as a control was deformed. This was the boundary of the non-thermal treatment. At 200 Hz, the arrival of the next pulse occurred after 5 ms, which is much longer than the relaxation time of the discharge current and voltage after the passage of the first pulse observed in the diagram. Further studies were carried out with the following selected optimal parameters: a gas pressure of 6 mTorr, a pulse repetition frequency of 200 Hz, a pulse duration of 20 μ S, and a voltage amplitude of 20 kV.

A calibration of the ion fluence based on previous results was performed using the UV absorption spectra of the PE film. For this purpose, PE films 20 μ m thick were treated with nitrogen ions of 20 keV energy, as it was conducted previously with ion beam treatment and with PIII of PE [47]. The UV spectra of PE and absorption at selected wavelengths as a function of treatment time are shown in Figure 2.

The UV absorption spectra of the treated PE samples showed increasing absorption with treatment time, similar to the previously observed absorption of PE films after ion beam treatment and PIII. The absorption in the short-wavelength region of the spectrum increases faster than in the long-wavelength region of the spectrum. The dependence of absorption on treatment time shows that an increase in light absorption occurs along an asymptotic curve with saturation. Saturated values of absorption correspond to the maximum degree of carbonisation of the surface layer of the PE, with the thickness corresponding to the penetration depth of the bombarding ions.

The results of the absorption in PE films, depending on the treatment time, were matched with the calibration curve obtained by treating the same PE films with nitrogen ions of 20 keV energy in an ion implanter with a known treatment fluence. This made it possible to interpret further results in the new system in terms of fluence, that is, 2×10^{13} ions arriving per 1 cm² surface area of the polymer per 1 s of the treatment.

To confirm the carbonisation of the PE surface in this treatment, micro-Raman spectra of the surface layer of PE were recorded (Figure 3). The spectrum shows the presence of D-peak at 1355 cm⁻¹ and G-peak at 1534 cm⁻¹ of the carbonised structure. According to the Raman model of the carbon spectrum [63], the ratio of peak intensities and their positions correspond to the nc-graphite phase with the amorphous carbon phase. The L_a cluster diameter is about 5 nm. A similar structure in the surface layer was observed after PIII and ion beam treatment of PE.

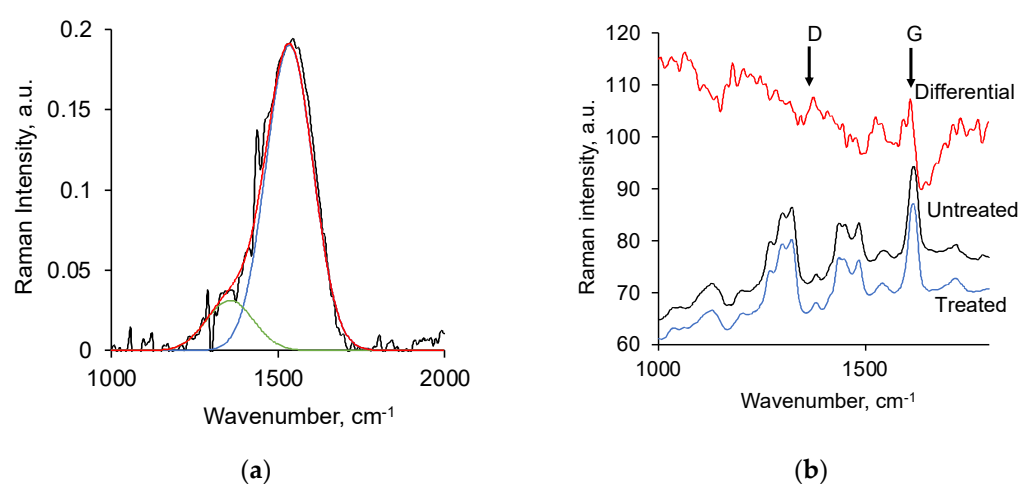


Figure 3. Micro-Raman spectra of (a) PE treated by an ion beam, black line is the experimental spectrum, green line is D-peak, blue line is G-peak, red is their sum; (b) untreated PU, treated PU by an ion beam and their difference.

Thus, the present plasma system creates a carbonised layer on the surface of PE films similar to the carbonised layer resulting from PIII and ion beam treatment in ion implanters.

This plasma system and optimal parameters for the non-thermal regime of treatment were used to activate the surface of medical PU for protein adsorption.

3.2. Ion Beam Treatment of Polyurethane

The surface of the PU film is smooth after the synthesis (Figure 4). The morphology of the untreated PU surface is mirrored by the surface profile of the substrate on which the PU film is formed. The treated PU surface is covered with cracks. PU is a highly elastic material and has an elongation at a break of 300% [60]. Therefore, the appearance of cracks on the surface of the treated PU indicates the formation of a brittle layer and internal stresses in it.

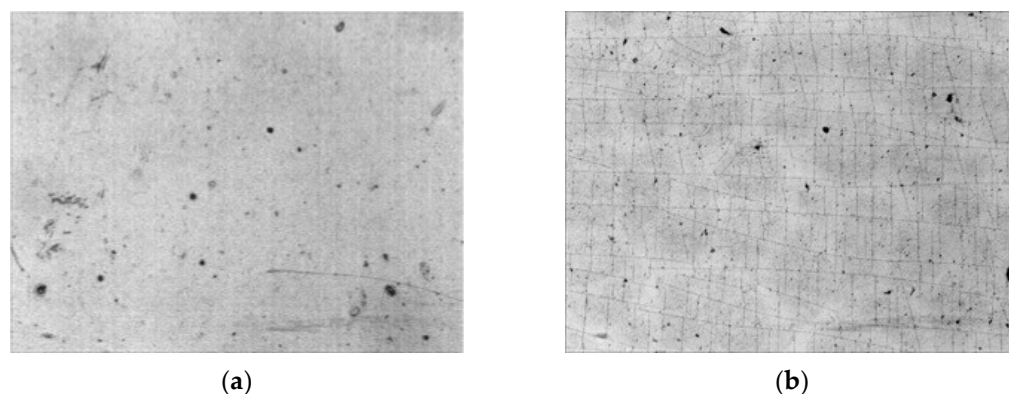


Figure 4. Micro-photo of: (a) untreated PU film; (b) PU film treated by ion beam. The size of both images is 1.2 mm × 0.9 mm.

The ellipsometry spectra and the subsequent optical model showed that the top surface layer of the treated PU has different optical parameters than the original untreated PU (Figure 5). The spectra of the original PU show some dispersion of the refractive index and extinction coefficient in the region of wavelengths shorter than 300 nm. This dispersion is due to the absorption of light in the aromatic structures and carbonyl groups of the PU. The refractive index values are in the region of about $n = 1.5$, which is typical for polymer materials, including polyurethane materials.

The refractive index of the surface layer of the treated PU is higher than that of the original PU. The extinction coefficient of this layer also shows increased values compared to the extinction coefficient of untreated PU.

The extinction coefficient spectra of PU show the same character as the UV absorption spectra for the treated PE. An increase in light absorption is observed higher in the short-wavelength region of the spectrum and lower in the long-wavelength region of the spectrum. This dispersion of the refractive index and extinction coefficient cannot be explained by the aromatic structures and carbonyl groups of the PU itself but can be explained by the formation of condensed aromatic rings and unsaturated carbon–carbon structures with various conjugation lengths.

The refractive index and extinction coefficient of the top layer increase with an increase in ion fluence. The increase has a saturation character. The saturated values are achieved for the treatment time above 400 s. A further increase in the treatment time does not increase the saturated values of the refractive index and extinction coefficient. The refractive index value reaches $n = 1.8$, which is typical for the refractive index of carbon film in the form of graphite or diamond [64,65].

The thickness of the modified top surface layer of PU, according to ellipsometry data, is about 30 nm. The thickness of the layer does not depend on the treatment time. At a treatment time of 40 s, the layer size is measured about 60 nm. However, the optical model of this sample does not fit the experimental curves well. The refractive index and extinction coefficient spectra have deviations, which can be associated with the inhomogeneity of the modified layer at low treatment time. Therefore, the optical model of ellipsometry spectra

for these samples, consisting of two homogeneous materials, is not correct. Unfortunately, it was also not possible to obtain a sufficiently accurate optical model with an effective layer for these samples.

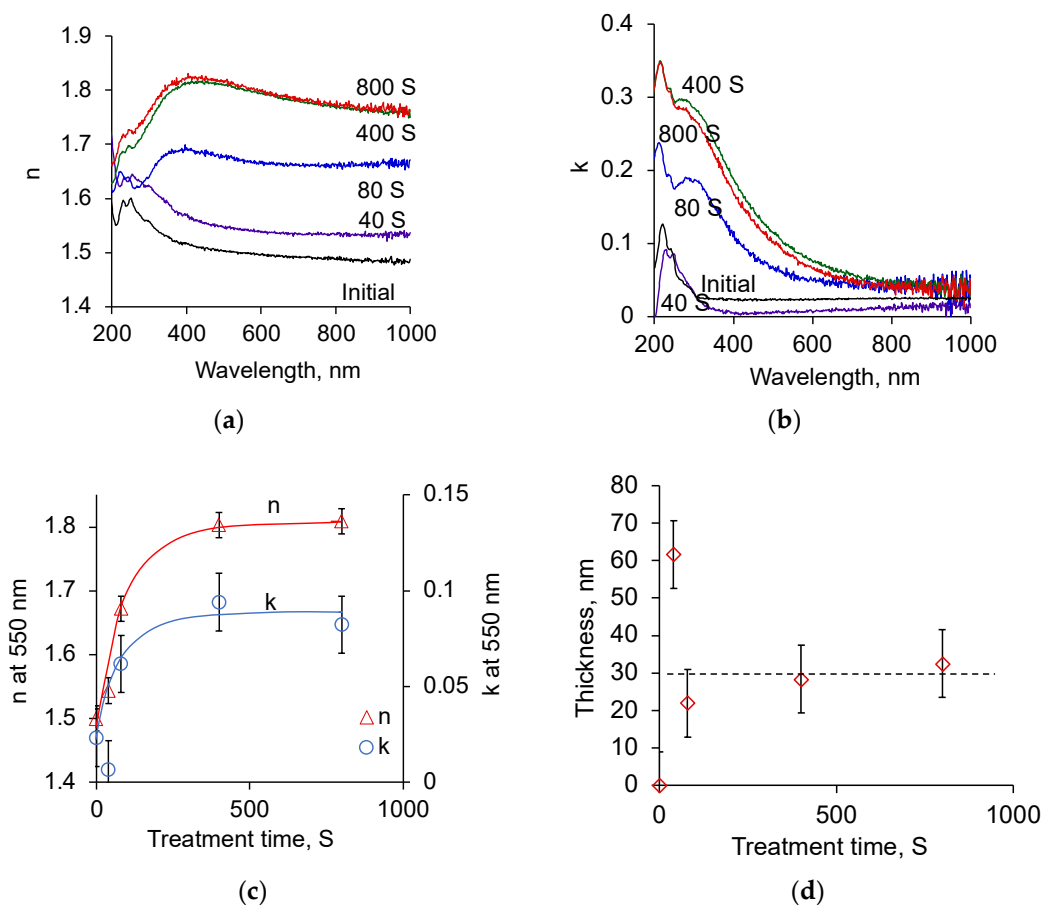


Figure 5. Optical ellipsometry spectra and results of ion beam treated PU: (a) spectra of the refractive index of the top layer for different treatment time (marked in s); (b) spectra of the extinction coefficient of the top layer for different treatment time (marked in s); (c) refractive index and extinction coefficient of the top layer in dependence on treatment time; (d) thickness of the top layer in dependence on treatment time.

XPS spectra of untreated PU showed the presence of carbon (78.1%), oxygen (19.0%), and nitrogen (2.9%) in the ester, urea, and urethane bonds (Figure 6). The relative concentration of these elements, calculated by the integral intensity of the lines, corresponds to the structural formula of PU.

The spectra of the treated PU showed significant differences. The total nitrogen content increased, and the total oxygen content decreased markedly (Figure 7). The total carbon content did not change, but the carbon content in the carbon–carbon bonds increased from 51.5% to 62.4%. The ether groups' carbon and oxygen content decreased significantly (Figure 7). The carbon and oxygen content in carbonyl groups increased. New lines of nitrogen in unsaturated double (401.5 eV) and triple bonds (404.4 eV) with carbon atoms appeared. The concentration of elements, calculated by the intensity of these lines, no longer corresponded to the structural formula of PU.

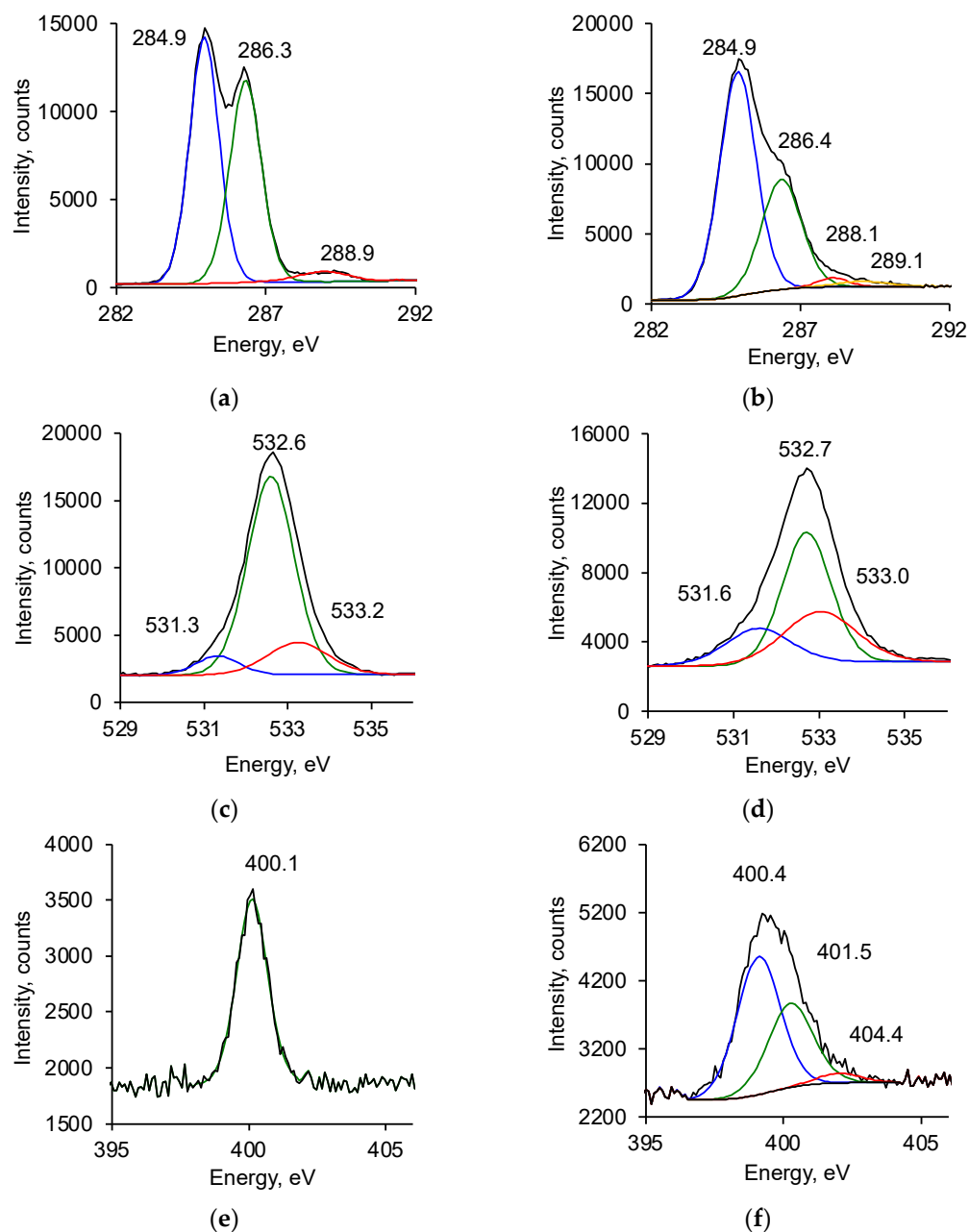


Figure 6. X-ray photoelectron spectra (XPS) of untreated (a,c,e) and treated (b,d,f) PU films: (a,b) C_{1s} region; (c,d) O_{1s} region; and (e,f) N_{1s} region. The experimental lines are fitted with Gauss functions (color lines). Position of maximum is marked in eV.

FTIR ATR spectra of untreated PU show lines of ester group, methyl groups, urethane, urea, and aromatic groups according to the structural formula of the PU (Figure 8). The spectra of the treated PU differ slightly in the region of $3700\text{--}3000\text{ cm}^{-1}$ and $1800\text{--}1500\text{ cm}^{-1}$. Small differences in the spectra are due to the fact that the thickness of the modified layer as a result of ion beam treatment (less than 100 nm) is significantly less than the thickness of the analysed layer in the FTIR ATR spectrum with ATR germanium crystal (400–600 nm). For a detailed analysis, differential spectra were obtained, where the spectrum of untreated PU was subtracted from the spectra of the treated PU. In the differential spectra, new lines are clearly visible in the region of vibrations of the hydroxyl group with maximum at 3480 and 3410 cm^{-1} , a complex contour in the region of vibrations of the $C=O$, $C=N$ and $C=C$ groups with maximum at 1703 cm^{-1} , 1670 cm^{-1} and a shoulder up to 1600 cm^{-1} , and an intense line in the region of $C-O$ vibrations with a maximum at 1080 cm^{-1} .

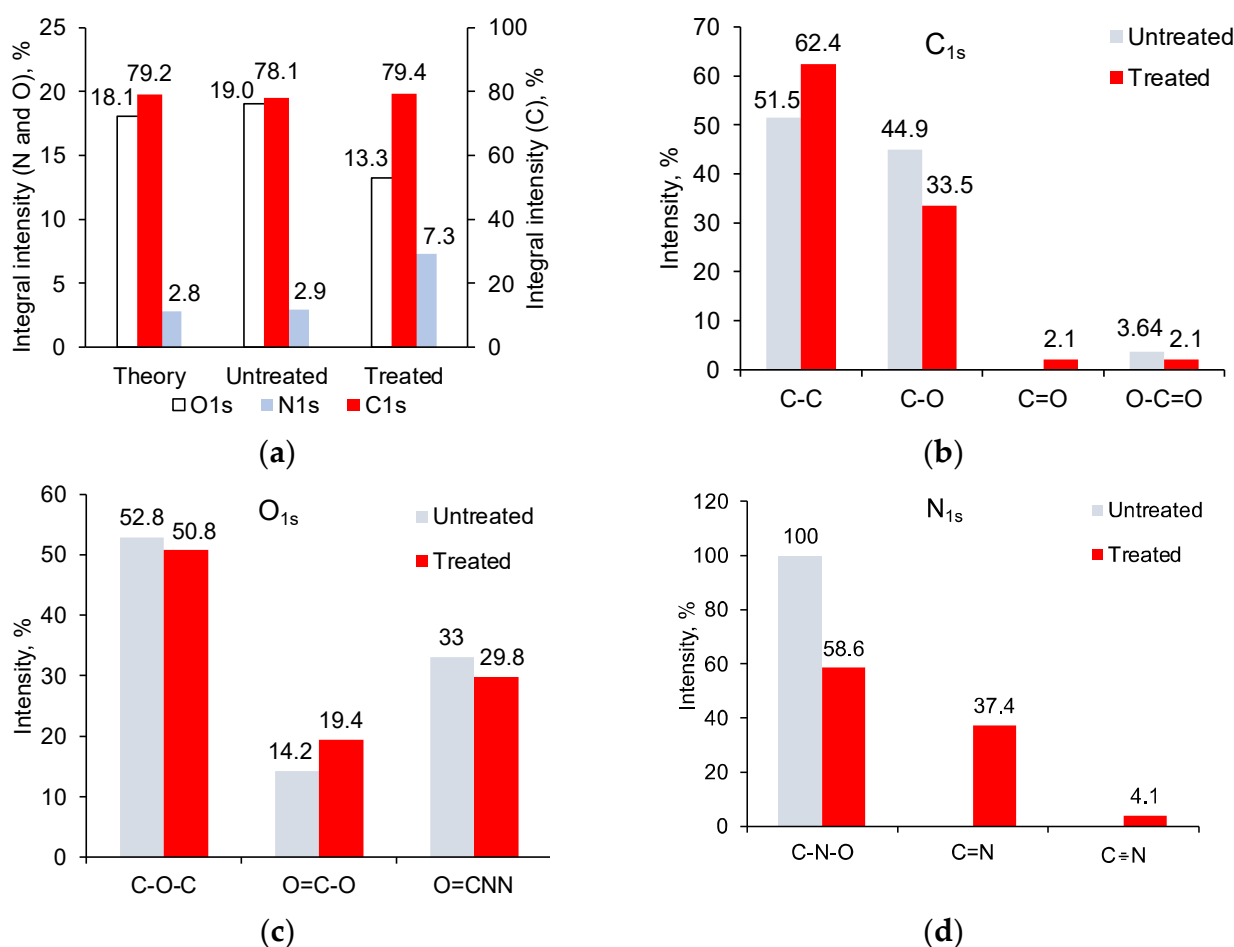
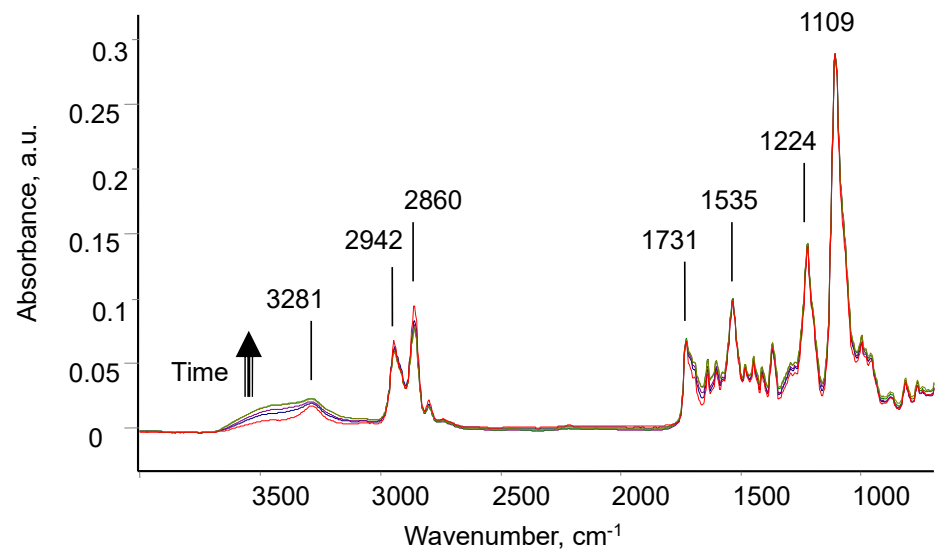


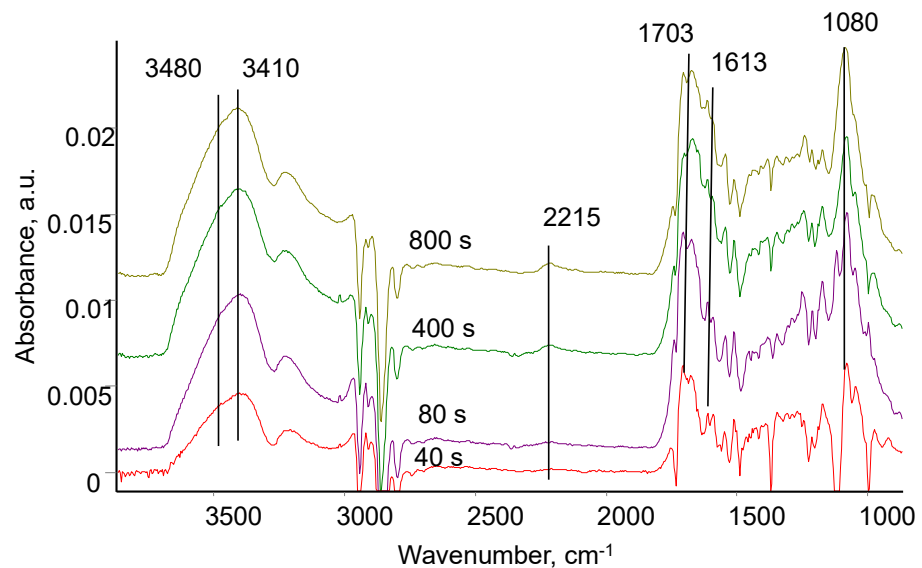
Figure 7. The element content of untreated and treated PU surface provided by XPS data: (a) total content; (b) content of carbon atoms in different bonds by high-resolution C1s line; (c) content of oxygen atoms in different bonds by high-resolution O1s line; and (d) content of nitrogen atoms in different bonds by high-resolution N1s line.

For quantitative measurements of spectral line intensity, the method of internal standard was used (Figure 9). For this purpose, the intensity of the 3410 cm^{-1} new vibration line of the hydroxyl group was normalised to the intensity of the 2859 cm^{-1} line of methyl groups of PU. The intensity of 1703 cm^{-1} , 1670 cm^{-1} , and 1613 cm^{-1} new vibration lines of unsaturated groups was normalised to the intensity of line 1534 cm^{-1} vibrations of Amide II of PU. This intensity normalisation made it possible to take into account the quality of the optical contact of the PU sample with the ATR crystal. For all new lines analysed, an asymptotic dependence of the intensity of these lines on the treatment time was observed. After 400 s of treatment, the increase in the intensity of new lines practically stopped within the standard deviation range.

Raman spectra of PU also showed the formation of a carbonised structure in the surface layer of PU after the treatment (Figure 3). However, in contrast to the Raman spectrum of treated PE, the intensity of the new lines of the carbonised structure in the spectrum of treated PU is low. Observation of the lines of the carbonised structure was possible only in the differential Raman spectrum. The D-line is observed at 1378 cm^{-1} , and the G-line is observed at 1610 cm^{-1} . The position of these lines and the ratio of their intensities indicate the presence of nc-graphite of 2 nm characteristic size in the surface layer of the treated PU.



(a)



(b)

Figure 8. FTIR ATR spectra of PU films treated with treatment different times: (a) original spectra, spectral change with treatment time is shown with array; (b) differential spectra (spectrum of untreated PU is subtracted). Different color lines correspond to different treatment time.

The ion beam treatment also changed the water wetting of the PU (Table 1). Untreated PU showed a water contact angle of 94 degrees. The contact angle of the treated PU immediately after removing the sample from the vacuum chamber to the air was 37 degrees. But after a month, the contact angle increased to 57 degrees. The contact angle of the non-polar liquid methyl diiodide was 55 degrees for untreated PU, 39 degrees for freshly treated PU, and 50 degrees for treated PU after long-term storage. Thus, the contact angles of the treated PU did not return to the original values for the untreated PU.

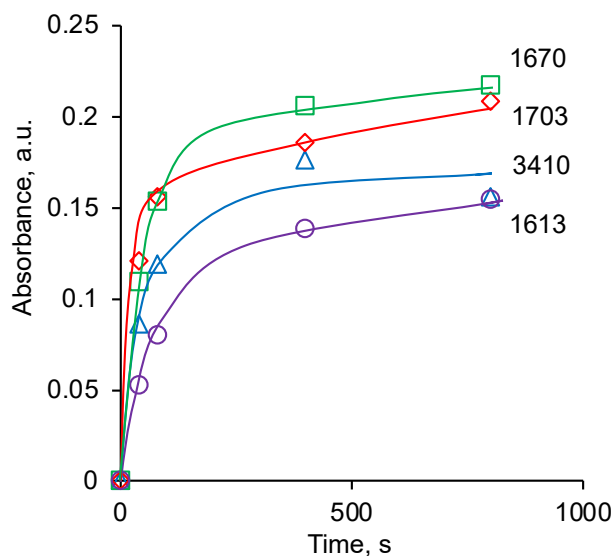


Figure 9. The absorbance of spectral lines in the FTIR ATR spectra of PU depends on treatment time.

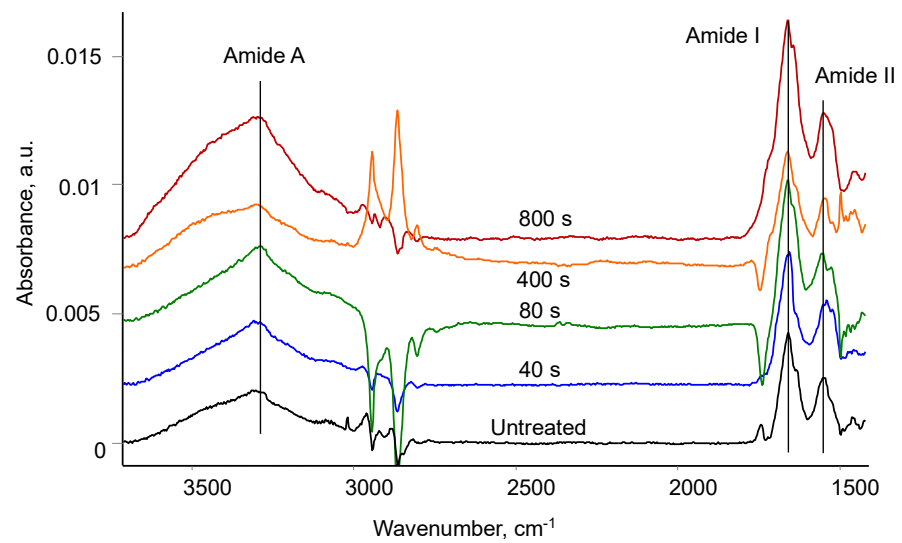
Table 1. Wetting contact angles (degree) and surface energy (mJ/m²) of PU untreated and ion beam treated of 800 s.

Title 1	Title 2			Title 3	
	Water	CH ₂ I ₂	Total	Polar	Dispersic
Untreated	94	55	32.6	1.2	31.4
Treated after 30 min	37	39	65.4	25.3	40.1
Treated, after 1 month	57	50	50.6	16.4	34.3

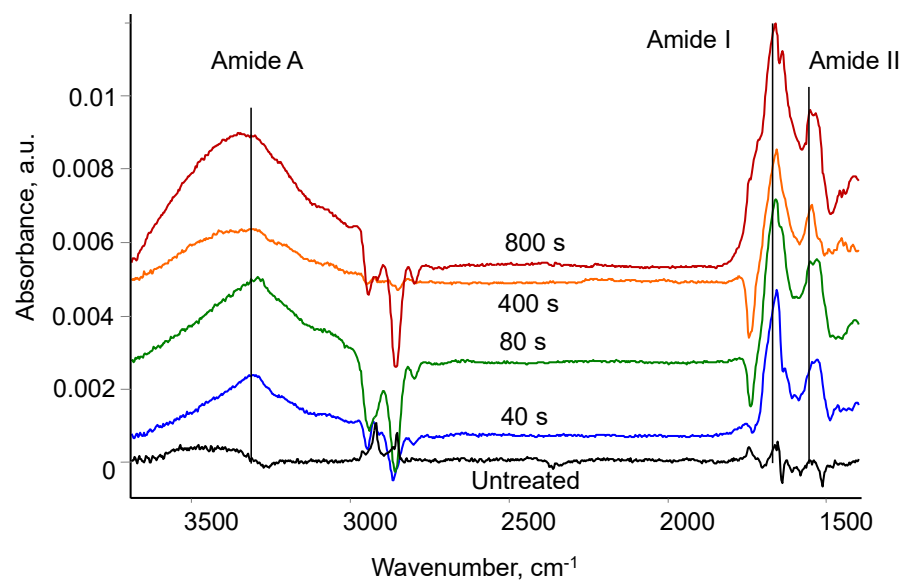
The surface energy and its polar and dispersic components, as calculated by the Owens–Wendt method, showed that the untreated PU surface is highly hydrophobic. The total surface energy of 32.6 mJ/m² is mainly formed by a dispersic component of 31.4 mJ/m². The polar component of 1.2 mJ/m² is neglectable. After the ion beam treatment, the surface energy increases to 65.4 mJ/m² due to the most change in the polar component of 25.3 mJ/m². After a month of storage time, the total surface energy drops to 50.6 mJ/m², with the polar component decreasing to 16.4 mJ/m² the most. Thus, the surface energy of ion beam-treated PU remains sufficiently high after a long storage time.

3.3. Attachment of Fibrinogen

The FTIR ATR spectra of PU with fibrinogen coating differ very little from the spectra of the same PU samples without fibrinogen. The intensity of fibrinogen vibration lines cannot be visibly high if the fibrinogen layer is a monolayer. To analyse the spectrum of the applied fibrinogen, the differential spectra of PU were obtained. The spectrum of PU without protein was subtracted from the spectrum of PU with attached fibrinogen. In this case, the conditions and time for ion beam treatment of the PU, the time after ion beam treatment until the application of the fibrinogen solution, the conditions for keeping the PU in a buffer solution, the conditions and time for washing unbound protein in buffer, water, and detergent, the conditions and time for drying the samples were identical for the sample with fibrinogen and a sample without protein. Then, the spectrum of the PU vibrations is subtracted completely, allowing the spectrum of the adsorbed fibrinogen to be clearly observed. The differential spectra of PU with attached fibrinogen are shown in Figure 10.



(a)



(b)

Figure 10. Differential spectra of PU surface with attached fibrinogen: (a) fibrinogen is attached and washed in the buffer; (b) fibrinogen is attached and washed with detergent. The spectrum of PU is subtracted. The treatment time of polyurethane in an ion beam is shown.

The spectra are shown for samples of untreated PU and for PU treated with different treatment times. The spectral lines of Amide A at 3300 cm^{-1} , Amide I at 1650 cm^{-1} and Amide II at 1540 cm^{-1} as the characteristic vibrations of the amide group in the fibrinogen molecule are clearly observed. The intensity of the fibrinogen lines is much lower than the intensity of the vibration lines of the PU itself and the carbonised surface layer. The fibrinogen spectra look the same for all PU samples, untreated and treated with an ion beam: the position of the lines and the ratio of their intensities do not differ. These spectra refer to the fibrinogen physically and chemically adsorbed on the surface of the PU.

Differential spectra of PU after washing in detergent showed the presence of fibrinogen lines for samples treated with an ion beam only (Figure 10). In the spectra of these samples, the lines Amide A at 3300 cm^{-1} , Amide I at 1650 cm^{-1} , and Amide II at 1540 cm^{-1} are

visible. In the spectrum of untreated PU, no lines are observed in these regions at the noise level of the spectrum.

To quantify the fibrinogen on the PU surface, the peak intensity of all Amide lines was used. The intensity of the lines was normalised to known extinction coefficients for each individual Amide line determined earlier [48]. After the normalisation, the intensities of all Amide lines were averaged. The results are presented in Figure 11. The averaged values are proportional to the relative concentration of the fibrinogen according to the Bouguer–Lambert law. The concentration of fibrinogen attached to the surface of untreated PU is about half of the concentration of fibrinogen attached to the surface of ion beam-treated PU. The concentration of the attached fibrinogen does not depend on the ion beam treatment time.

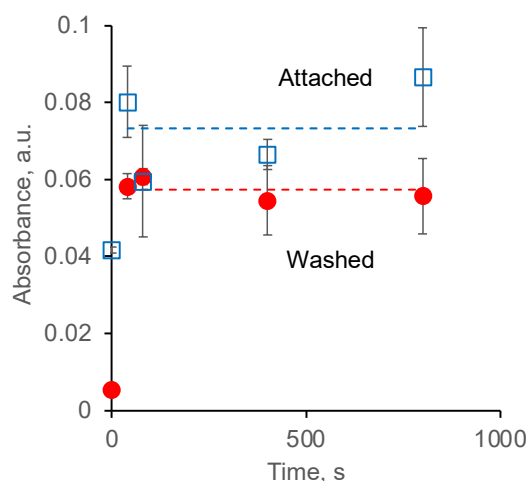


Figure 11. The absorbance of fibrinogen lines in FTIR ATR spectra of PU with attached fibrinogen before and after washing in detergent.

The fibrinogen was completely washed out from the surface of untreated PU in detergent, which is observed by the absence of the Amide lines in the spectrum. The concentration of fibrinogen remaining on the surface of the ion beam treated PU after washing in detergent is, on average, about 80% of the concentration of initially attached fibrinogen. The remaining fibrinogen concentration after washing does not depend on the ion beam treatment time.

4. Discussion

The results of medical PU treatment using a new plasma system showed that, despite the simplification of the system and treatment process, the activation of the PU surface occurs in approximately the same way as in the case of ion beam treatment and PIII. A layer of carbonised structures, such as condensed aromatic clusters, is formed on the surface, in which the carbon atoms at the edges of the clusters have unpaired electrons. This is observed in the Raman and UV absorption spectra. The characteristic sizes of these clusters, in this case, were 2 nm. For comparison, the size of clusters on the surface of PE treated with nitrogen ions with an energy of 20 keV in ion beam treatment was 2 nm. The sizes of clusters formed as a result of PIII treatment on the surface of polystyrene treated with argon ions with an energy of 20 keV are 1 nm and nitrogen ions with an energy of 20 keV 1.8 nm. The sizes of graphite clusters on the surface of Pebax polyamide treated in PIII with nitrogen ions with an energy of 20 keV were 1.5 nm, and with an energy of 30 keV, they were 1.8 nm [47]. The sizes of graphite clusters on the surface of PU treated in PIII with nitrogen ions with an energy of 20 keV were 2.5 nm [49]. The size of graphitic clusters is important for the stabilisation of free radicals in the surface layer after ion beam treatment before a protein solution is applied.

The graphitic clusters that appear in the surface layer of PU contain free radicals. The ESR spectra of the treated PU showed the appearance of unpaired electrons at carbon atoms located in the graphite clusters. Similar signals of unpaired electrons in graphite clusters were observed in PU [49], polyether ether ketone, and PE [48] treated by nitrogen ions in PIII. In this case, the signal of unpaired electrons in the EPR spectra was observed after long-term exposure of the treated PU to air at room temperature. This also corresponds to the literature data on the stabilisation of free radicals at the edges of graphite clusters [66–69].

In the FTIR ATR spectra of treated PU, rather strong lines of hydroxyl groups are observed. Similar lines were observed in the spectra of PU treated with PIII with nitrogen ions with an energy of 20 keV. These changes correspond to the depolymerisation of the deep layers that lie beneath the surface carbonised layer. This process is apparently caused by the migration of free radicals from the surface carbonised layer into the deeper native layers of the PU.

At the same time, it is necessary to note a much lower degree of carbonisation of the surface layer of PU in this treatment method. Under the same treatment conditions (energy and type of ions, ion fluence), a significantly smaller thickness of the carbonised layer (30 nm) is observed in this method compared to PIII, where the thickness of the carbonised layer is about 70 nm. According to SRIM calculations, the penetration depth of nitrogen ions with an energy of 20 keV is about 70 nm. Therefore, the difference in the depth of penetration of nitrogen ions into PU and the thickness of the resulting carbonised layer of PU remains unclear.

The graphitic clusters with free radicals that appeared on the surface provided a covalent attachment of fibrinogen molecules to the surface of the treated PU. Washing the non-covalently grafted fibrinogen from the surface with a detergent showed that the fibrinogen from the surface of the untreated PU is washed off almost completely, while about 80% of the initially adsorbed fibrinogen remains on the treated PU.

Similar adsorbed protein retention results were observed on other polymers treated with PIII [47,48]. It was shown that after treatment, a continuous monolayer of protein is formed on the surface of the treated polymers. Drawing parallels with previous results, it can be assumed that this treatment also provides a protein coating on the total surface of the treated PU.

Thus, we can assume that this type of treatment can be used to activate the surface of PU for biomedical applications such as non-rejected implants [49], microarray for analysis, improved cell adhesion devices [46], and other biomedical devices where the covalent adsorption of protein onto the surface is a key factor. The precursors for protein covalent attachment are not required. The plasma system has a simple design and can be directly installed in a biomedical laboratory or surgery room. Following studies with animal trials are on the way.

5. Conclusions

A simple and efficient system has been created for ion beam treatment of the polymer surface. The system consists of a vacuum chamber with a high-voltage electrode and a pulse generator. This system does not require additional plasma generation in the chamber to produce the ion beam. These studies have shown that the biomedical polyurethane treated by an ion beam contains the active surface layer. The layer is characterised by carbonised structures consisting of condensed aromatic rings, partially depolymerised underneath the layer with hydroxyl groups and high surface energy. The modified surface layer totally lost the initial polyurethane chemical structure after a fluence of 10^{16} ions/cm². The surface layer thickness is observed to be less than the penetration depth of nitrogen ions with 20 keV energy. The surface is not stable and changes with storage time after the treatment. This system activates the polyurethane surface with free radicals on the edge of graphitic clusters which can covalently graft a protein onto the polyurethane with complete coverage of the polymer surface without precursors. The highest activity of the treated surface to attach protein is expected straight after the treatment. The system can be

directly installed in a biomedical laboratory or surgery room to activate the polyurethane biomedical device before usage. Future investigations with animal trials are on the way.

Author Contributions: Conceptualisation: V.C. and A.K.; investigation: V.C. and A.K.; writing: V.C. and A.K.; supervision: I.S. and I.K. All authors have read and agreed to the published version of the manuscript.

Funding: This research was funded by the Government of the Perm Krai, grant number C-26/875.

Institutional Review Board Statement: The study did not require ethical approval.

Data Availability Statement: Data are available on request from the corresponding author.

Acknowledgments: The author (VC) thanks M. Bilek and D. McKenzie for their support and permission to conduct a part of this study in their laboratory.

Conflicts of Interest: The authors declare no conflicts of interest. The funders had no role in the design of this study; in the collection, analyses, or interpretation of data; in the writing of the manuscript; or in the decision to publish the results.

References

- Mariani, E.; Lisignoli, G.; Borzi, R.M.; Pulsatelli, L. Biomaterials: Foreign Bodies or Tuners for the Immune Response? *Int. J. Mol. Sci.* **2019**, *20*, 636. [[CrossRef](#)] [[PubMed](#)]
- Ward, W.K. A Review of the Foreign-body Response to Subcutaneously-implanted Devices: The Role of Macrophages and Cytokines in Biofouling and Fibrosis. *J. Diabetes Sci. Technol.* **2008**, *2*, 768–777. [[CrossRef](#)]
- Kizhakkedathu, J.N.; Conway, E.M. Biomaterial and cellular implants: Foreign surfaces where immunity and coagulation meet. *Blood* **2022**, *139*, 1987–1998. [[CrossRef](#)] [[PubMed](#)]
- Tang, L.; Eaton, J. Natural Responses to Unnatural Materials: A Molecular Mechanism for Foreign Body Reactions. *Mol. Med.* **1999**, *5*, 351–358. [[CrossRef](#)]
- Schmid, A.; Dordick, J.S.; Hauer, B.; Kiener, A.; Wubbolts, M.; Witholt, B. Industrial biocatalysis today and tomorrow. *Nature* **2001**, *409*, 258–268. [[CrossRef](#)]
- Hu, W.-J.; Eaton, J.W.; Tang, L. Molecular basis of biomaterial-mediated foreign body reactions. *Blood* **2001**, *98*, 1231–1238. [[CrossRef](#)]
- Castner, D.G.; Ratner, B.D. Biomedical surface science: Foundations to frontiers. *Surf. Sci.* **2002**, *500*, 28–60. [[CrossRef](#)]
- Ottenbrite, R.M. (Ed.) *Frontiers in Biomedical Polymer Applications*; Technomic Publishing Company: Lancaster, UK, 1998.
- Ryan, B.J.; Carolan, N.; Fagain, C. Horseradish and soybean peroxidases: Comparable tools for alternative niches? *Trends Biotechnol.* **2006**, *24*, 355–363. [[CrossRef](#)] [[PubMed](#)]
- Boecking, T.; James, M.; Coster, H.G.L.; Chilcott, T.C.; Barrow, K.D. Structural Characterization of Organic Multilayers on Silicon (111) formed by Immobilization of Molecular Films on Functionalized Si-C Linked Monolayers. *Langmuir* **2004**, *20*, 9227–9235. [[CrossRef](#)]
- Williams, R.A.; Blanch, H.W. Covalent Immobilization of Protein Monolayers for Biosensor Applications. *Biosens. Bioelectron.* **1994**, *9*, 159–167. [[CrossRef](#)]
- Peterman, J.H.; Tarcha, P.J.; Chu, V.P.; Butler, J.E. The immunochemistry of sandwich-ELISAs IV. The Antigen Capture Capacity of Antibody Covalently Attached to Bromoacetyl Surface-Functionalized Polystyrene. *J. Immunol. Methods* **1988**, *111*, 271–275. [[CrossRef](#)] [[PubMed](#)]
- Cunha, A.G.; Fernández-Lorente, G.; Bevilaqua, J.V.; Destain, J.; Paiva, L.M.C.; Freire, D.M.G.; Fernández-Lafuente, R.; Guisán, J.M. Immobilization of *Yarrowia lipolytica* lipase—a comparison of stability of physical adsorption and covalent attachment techniques. *Appl. Biochem. Biotechnol.* **2008**, *146*, 49–56. [[CrossRef](#)] [[PubMed](#)]
- Gan, S.Y.; Tye, G.J.; Chew, A.L.; Ng, W.K.; Lai, N.S. Linker-mediated oriented antibody immobilisation strategies for a more efficient immunosensor and diagnostic applications: A review. *Biosens. Bioelectron.* **2023**, *14*, 100379. [[CrossRef](#)]
- Abbas, M.; Torati, S.R.; Kim, C.G. Multifunctional Fe₃O₄/Au core/satellite nanocubes: An efficient chemical synthesis, characterization and functionalization of streptavidin protein. *Dalton Trans.* **2017**, *46*, 2303–2309. [[CrossRef](#)]
- Baldini, F.; Carloni, A.; Giannetti, A.; Porro, G.; Trono, C. An optical PMMA biochip based on fluorescence anisotropy: Application to C-reactive protein assay. *Sens. Actuators* **2009**, *139*, 64–68. [[CrossRef](#)]
- Bhardwaj, H.; Sumana, G.; Marquette, C.A. A label-free ultrasensitive microfluidic surface Plasmon resonance biosensor for Aflatoxin B1 detection using nanoparticles integrated gold chip. *Food Chem.* **2020**, *307*, 125530. [[CrossRef](#)] [[PubMed](#)]
- Ricci, S.; Casalini, S.; Parkula, V.; Selvaraj, M.; Saygin, G.D.; Greco, P.; Biscarini, F.; Mas-Torrent, M. Label-free immunodetection of α -synuclein by using a microfluidics coplanar electrolyte-gated organic field-effect transistor. *Biosens. Bioelectron.* **2020**, *167*, 112433. [[CrossRef](#)] [[PubMed](#)]
- Merker, D.; Bertinetti, D.; Merz, R.; Kopnarski, M.; Herberg, F.W.; Popov, C. Enhanced protein immobilization efficacy by nanostructuring of ultrananocrystalline diamond surface. *Diam. Relat. Mater.* **2023**, *136*, 109898. [[CrossRef](#)]

20. Wang, Y.; Zhang, X.; Han, N.; Wu, Y.; Wei, D. Oriented covalent immobilization of recombinant protein A on the glutaraldehyde activated agarose support. *Int. J. Biol. Macromol.* **2018**, *120*, 100–108. [[CrossRef](#)]
21. Chen, W.-C.; Chen, Y.-S.; Chang, K.-C.; Chen, C.-H.; Li, D.-J. An in vitro assessment and comparative effectiveness of silanized-glutaraldehyde functionalized titanium surfaces with phosphatidylcholine and type I collagen grafts. *Dent. Mater.* **2020**, *36*, 320–328. [[CrossRef](#)]
22. de Andrades, D.; Graebin, N.G.; Kadowaki, M.K.; Ayub, M.A.Z.; Fernandez-Lafuente, R.; Rodrigues, R.C. Immobilization and stabilization of different β -glucosidases using the glutaraldehyde chemistry: Optimal protocol depends on the enzyme. *Int. J. Biol. Macromol.* **2019**, *129*, 672–678. [[CrossRef](#)] [[PubMed](#)]
23. Baranowska, M.; Slota, A.J.; Eravuchira, P.J.; Alba, M.; Formentin, P.; Pallarès, J.; Ferré-Borrull, J.; Marsal, L.F. Protein attachment to silane-functionalized porous silicon: A comparison of electrostatic and covalent attachment. *J. Colloid Interface Sci.* **2015**, *452*, 180–189. [[CrossRef](#)] [[PubMed](#)]
24. Stachelek, S.J.; Finley, M.J.; Alferiev, I.S.; Wang, F.; Tsai, R.K.; Eckells, E.C.; Tomczyk, N.; Connolly, J.M.; Discher, D.E.; Eckmann, D.M.; et al. The effect of CD47 modified polymer surfaces on inflammatory cell attachment and activation. *Biomaterials* **2011**, *32*, 4317–4326. [[CrossRef](#)]
25. Fink, D. *Fundamentals of Ion-Irradiated Polymers*; Springer: Berlin/Heidelberg, Germany, 2004.
26. Odzhaev, V.B.; Kozlov, I.P.; Popok, V.N.; Sviridov, D.B. *Ion Implantation of Polymers*; Belorussian State University: Minsk, Belorussia, 1998.
27. Bačáková, L.; Švorčík, V.; Rybka, V.; Miček, I.; Hnatowicz, V.; Lisá, V.; Kocourek, F. Adhesion and proliferation of cultured human aortic smooth muscle cells on polystyrene implanted with N^+ , F^+ and Ar^+ ions: Correlation with polymer surface polarity and carbonization. *Biomaterials* **1996**, *17*, 1121–1126. [[CrossRef](#)] [[PubMed](#)]
28. Calcagno, L.; Compagnini, G.; Foti, G. Structural modification of polymer film by ion irradiation. *Nucl. Instr. Meth.* **1992**, *62*, 413–422. [[CrossRef](#)]
29. Davenas, J.; Thevenard, P.; Boiteux, G.; Fallavier, M.; Lu, X.L. Hydrogenated carbon layers produced by ion beam irradiation of PMMA and polystyrene films. *Nucl. Instrum. Meth. Phys. Res.* **1990**, *46*, 317–323. [[CrossRef](#)]
30. Tóth, A.; Bell, T.; Bertóti, I.; Mohai, M.; Zelei, B. Surface modification of polyethylene by low keV ion beams. *Nucl. Instrum. Methods Phys. Res.* **1999**, *148*, 1131–1135. [[CrossRef](#)]
31. Lee, J.-S.; Kaibara, M.; Iwaki, M.; Sasabe, H.; Suzuki, Y.; Kusakabe, M. Selective adhesion and proliferation of cells on ion-implanted polymer domains. *Biomaterials* **1993**, *14*, 958. [[CrossRef](#)] [[PubMed](#)]
32. Melnig, V.; Apetroaei, N.; Dumitrascu, N.; Suzuki, Y.; Tura, V. Improvement of polyurethane surface biocompatibility by plasma and ion beam techniques. *J. Optoelectron. Adv. Mater.* **2005**, *7*, 2521–2528.
33. Marletta, G. Ion-beam modification of polymer surfaces for biological applications. In *Materials Science with Ion Beams*; Bernas, H., Ed.; Springer: Berlin/Heidelberg, Germany, 2010; pp. 345–371.
34. Fu, R.K.Y.; Cheung, I.T.L.; Mei, Y.F.; Shek, C.H.; Siu, G.G.; Chu, P.K.; Yang, W.M.; Leng, Y.X.; Huang, Y.X.; Tian, X.B.; et al. Surface modification of polymeric materials by plasma immersion ion implantation. *Nucl. Inst. Meth. Phys. Res.* **2005**, *237*, 417–421. [[CrossRef](#)]
35. Kostov, K.G.; Ueda, M.; Tan, I.H.; Leite, N.F.; Beloto, A.F.; Gomes, G.F. Structural effect of nitrogen plasma-based ion implantation on ultra-high molecular weight polyethylene. *Surf. Coat. Technol.* **2004**, *186*, 287–290. [[CrossRef](#)]
36. Sahre, K.; Eichhorn, K.-J.; Simon, F.; Pleul, D.; Janke, A.; Gerlach, G. Characterization of ion-beam modified polyimide layers. *Surf. Coat. Technol.* **2001**, *139*, 257–264. [[CrossRef](#)]
37. Wong, K.H.; Zinke-Allmang, M.; Wan, W.K.; Zhang, J.Z.; Hu, P. Low energy oxygen ion beam modification of the surface morphology and chemical structure of polyurethane fibers. *Nucl. Inst. Meth. Phys. Res.* **2006**, *243*, 63–74. [[CrossRef](#)]
38. Popok, V. Ion implantation of polymers: Formation of nanoparticulate materials. *Rev. Adv. Mater. Sci.* **2012**, *30*, 1–26.
39. Murphy, J.J.; Patel, M.; Powell, S.J.; Smith, P.F. Volatile evolution induced by energetic He^{++} ions in a poly(ester) based polyurethane. *Radiat. Phys. Chem.* **2002**, *63*, 101–108. [[CrossRef](#)]
40. Iwaki, M.; Nakao, A.; Kaibara, M.; Sasabe, H.; Kaneko, S.; Nakajima, H.; Suzuki, Y.; Kusakabe, M.; Fujihana, T. Ion bombardment into inner wall surfaces of tubes and their biomedical applications. *Nucl. Inst. Meth. Phys. Res.* **1995**, *106*, 618–623. [[CrossRef](#)]
41. Dejun, L.; Jie, Z.; Hanqing, G.; Mozhu, L.; Fuqing, D.; Qiqing, Z. Surface modification of medical polyurethane by silicon ion bombardment. *Nucl. Inst. Meth. Phys. Res.* **1993**, *82*, 57–62. [[CrossRef](#)]
42. Huang, N.; Yang, P.; Leng, Y.X.; Wang, J.; Sun, H.; Chen, J.Y.; Wan, G.J. Surface modification of biomaterials by plasma immersion ion implantation. *Surf. Coat. Technol.* **2004**, *186*, 218–226. [[CrossRef](#)]
43. Vyatkin, A.F.; Smirnov, V.V.; Kholopkin, A.I. Development of ion implantation equipment in the USSR. *Solid State Technol.* **1991**, *34*, 57. [[CrossRef](#)]
44. Begishev, V.; Gavrilov, N.; Mesyats, G.; Klyachkin, Y.; Kondyurina, I.; Osorgina, I.; Kondyurin, A. Modification of polyurethane endoprosthetics surface by pulse ion beam. In Proceedings of the 12th International Conference on High-Power Particle Beams, Haifa, Israel, 7–12 June 1998; Volume 2, pp. 997–1000.
45. Mesyats, G.; Klyachkin, Y.; Gavrilov, N.; Kondyurin, A. Adhesion of Polytetrafluorethylene modified by an ion beam. *Vacuum* **1999**, *52*, 285–289. [[CrossRef](#)]
46. Kondyurin, A.; Maitz, M.F. Surface Modification of ePTFE and Implants Using the Same. U.S. Patent WO2007/022174A3, 15 February 2007.

47. Kondyurin, A.; Bilek, M. Ion Beam Treatment of Polymers. In *Application Aspects from Medicine to Space*, 2nd ed.; Elsevier: Oxford, UK, 2014.
48. Kondyurin, A.V.; Naseri, P.; Tilley, J.M.R.; Nosworthy, N.J.; Bilek, M.M.M.; McKenzie, D.R. Mechanisms for Covalent Immobilization of Horseradish Peroxidase on Ion-Beam-Treated Polyethylene. *Scientifica* **2012**, *2012*, 126170. [[CrossRef](#)] [[PubMed](#)]
49. Kondyurina, I.; Kondyurin, A. Foreign Body Reaction (Immune Response) for Artificial Implants Can Be Avoided: An Example of Polyurethane in Mice for 1 Week. *J. Funct. Biomater.* **2023**, *14*, 432. [[CrossRef](#)] [[PubMed](#)]
50. Santos, S.G.; Lamghari, M.; Almeida, C.R.; Oliveira, M.I.; Neves, N.; Ribeiro, A.C.; Barbosa, J.N.; Barros, R.; Maciel, J.; Martins, M.C.L.; et al. Adsorbed fibrinogen leads to improved bone regeneration and correlates with differences in the systemic immune response. *Acta Biomater.* **2013**, *9*, 7209–7217. [[CrossRef](#)] [[PubMed](#)]
51. Balabiyev, A.; Podolnikova, N.P.; Kilbourne, J.A.; Baluch, D.P.; Lowry, D.; Zare, A.; Ros, R.; Flick, M.J.; Ugarova, T.P. Fibrin polymer on the surface of biomaterial implants drives the foreign body reaction. *Biomaterials* **2021**, *277*, 121087. [[CrossRef](#)] [[PubMed](#)]
52. Hu, W.; Wang, Y.; Chen, J.; Yu, P.; Tang, F.; Hu, Z.; Zhou, J.; Liu, L.; Qiu, W.; Ye, Y.; et al. Regulation of biomaterial implantation-induced fibrin deposition to immunological functions of dendritic cells. *Mater. Today Bio.* **2022**, *14*, 100224. [[CrossRef](#)] [[PubMed](#)]
53. Vilar, R.; Fish, R.J.; Casini, A.; Neerman-Arbez, M. Fibrin(ogen) in human disease: Both friend and foe. *Haematologica* **2020**, *105*, 284–296. [[CrossRef](#)] [[PubMed](#)]
54. Vasconcelos, D.M.; Gonçalves, R.M.; Almeida, C.R.; Pereira, I.O.; Oliveira, M.I.; Neves, N.; Silva, A.M.; Ribeiro, A.C.; Cunha, C.; Almeida, A.R.; et al. Fibrinogen scaffolds with immunomodulatory properties promote in vivo bone regeneration. *Biomaterials* **2016**, *111*, 163–178. [[CrossRef](#)] [[PubMed](#)]
55. Gavrilov, N.V.; Oks, E.M. High-current pulse sources of broad beams of gas and metal ions for surface treatment. *Nucl. Instrum. Methods Phys. Res.* **2000**, *439*, 31–44. [[CrossRef](#)]
56. Anders, A. (Ed.) *Handbook of Plasma Immersion Ion Implantation and Deposition*; Wiley: New York, NY, USA, 2000.
57. McKenzie, D.R.; Powles, R. Plasma Immersion Ion Implantation Using Conductive Mesh. US Patent 2007/0268089A1, 22 November 2007.
58. Osorgina, I.V.; Porozova, S.E.; Plaksin, S.A.; Morozov, I.A. Effect of Long-Term Exposure within the Body on the Condition of Polyurethane Membranes of Breast Prostheses. *Biomed. Eng.* **2016**, *50*, 63–66. [[CrossRef](#)]
59. Budnikov, V.I.; Begishev, V.P. Sanitary and chemical evaluation of polyester urethane elastomers. *Hyg. Sanit.* **1997**, *2*, 48–49.
60. Romanova, V.A.; Begishev, V.P. Regulating of properties of polymeric matrix on base of polyurethane at production of composites. *Compos. Mater. Constr.* **2006**, *4*, 39–43.
61. Ziegler, J.F.; Manoyan, J. The stopping of ions in compounds. *Nucl. Instr. and Meth.* **1998**, *35*, 215. [[CrossRef](#)]
62. Ziegler, J.F.; Biersack, J.P. *The Stopping and Range of Ions in Solid*; Pergamon: New York, NY, USA, 1985.
63. Ferrari, A.C.; Robertson, J. Interpretation of Raman spectra of disordered and amorphous carbon. *Phys. Rev.* **2000**, *61*, 14095–14107. [[CrossRef](#)]
64. Piazza, F.; Grambole, D.; Scheider, D.; Casiraghi, C.; Ferrari, A.C.; Robertson, J. Protective diamond-like carbon coatings for future optical storage disks. *Diamond Relat. Mater.* **2005**, *14*, 994–999. [[CrossRef](#)]
65. Stagg, B.; Charalampopoulos, T. Refractive index of pyrolytic graphite, amorphous carbon, and flame soot in the temperature range 25 to 600 °C. *Combust. Flame* **1993**, *94*, 381–396. [[CrossRef](#)]
66. Gambino, R.J.; Thompson, J.A. Spin resonance spectroscopy of amorphous carbon films. *Solid State Commun.* **1980**, *34*, 15–18. [[CrossRef](#)]
67. Fusco, G.; Tagliaferro, A.; Milne, W.I.; Robertson, J. Paramagnetic centres in tetrahedral amorphous carbon. *Diam. Relat. Mater.* **1997**, *6*, 783–786. [[CrossRef](#)]
68. Barklie, R.C. Characterisation of defects in amorphous carbon by electron paramagnetic resonance. *Diam. Relat. Mater.* **2001**, *10*, 174–181. [[CrossRef](#)]
69. Viana, G.A.; Lacerda, R.G.; Freire, F.L.; Marques, F.C. ESR investigation of graphite-like amorphous carbon films revealing itinerant states as the ones responsible for the signal. *J. Non-Cryst. Solids* **2008**, *354*, 2135–2137. [[CrossRef](#)]

Disclaimer/Publisher’s Note: The statements, opinions and data contained in all publications are solely those of the individual author(s) and contributor(s) and not of MDPI and/or the editor(s). MDPI and/or the editor(s) disclaim responsibility for any injury to people or property resulting from any ideas, methods, instructions or products referred to in the content.